ISSN 0036-0244, Russian Journal of Physical Chemistry A, 2014, Vol. 88, No. 13, pp. 2348–2358. © Pleiades Publishing, Ltd., 2014.

STRUCTURE OF MATTER AND QUANTUM CHEMISTRY

Theoretical Investigations on Nonlinear Optical and Spectroscopic Properties of 6-(3,3,4,4,4-Pentafluoro-2-hydroxy-1-butenyl)-2,4-pyrimidinedione: An Efficient NLO Material[1]

Hacer Pir Gümüs[a], Ömer Tamer[a]*, Davut Avci[a], Erdogan Tarcan[b], and Yusuf Atalay[a]

[a] *Sakarya University, Art and Science Faculty, Department of Physics, Sakarya, 54140 Turkey*

[b] *Kocaeli University, Art and Science Faculty, Department of Physics, Kocaeli, 41380 Turkey*

**e-mail: omertamer@sakarya.edu.tr*

Received October 28, 2013

Abstract—In this study, quantum chemical calculations of geometric parameters, conformational, natural bond orbital (NBO) and nonlinear optical (NLO) properties, vibrational frequencies, ^{1}H and ^{13}C NMR chemical shifts of the title molecule [$C_9H_7F_5N_2O_3$] in the ground state have been calculated with the help of Density Functional Theory (DFT–B3LYP/6-311++G(*d*,*p*)) and Hartree-Fock (HF/6-311++G(*d*,*p*)) methods. The optimized geometric parameters, vibrational frequencies, ^{1}H and ^{13}C NMR chemical shifts values are compared with experimental values of the investigated molecules. Comparison between experimental and theoretical results showed that B3LYP/6-311++G(*d*,*p*) method is able to provide more satisfactory results. In order to understand this phenomenon in the context of molecular orbital picture, we examined the molecular frontier orbital energies (HOMO, HOMO-1, LUMO, and LUMO + 1), the energy difference (ΔE) between E_{HOMO} and E_{LUMO}, electronegativity (χ), hardness (η), softness (S) calculated by HF/6-311++G(*d*,*p*) and B3LYP/6-311++G(*d*,*p*) levels. The molecular surfaces, Mulliken, NBO, and Atomic polar tensor (APT) charges of the investigated molecule have also been calculated by using the same methods.

Keywords: C-6 fluoroalkylated pyridine, potential energy scan, natural bonding orbital analysis, nonlinear optical properties, HF and DFT calculations.

DOI: 10.1134/S0036024414130068

INTRODUCTION

The excellent biological activities exhibited by 6-substituted uracil derivatives provide a new emphasis to explore the chemical and biological activities of these pyrimidine derivatives [1–6]. It was demonstrated that a large number of acyclic nucleoside analogues have antiviral activities against herpes viruses due to their selective and efficient activation through monophosphorylation by the viral enzyme in the intact cells [7, 8]. Additionally, it is well known that pyrimidines are biologically important molecules and have valuable heterocyclic nuclei for the design of pharmaceutical agents [6].

The title molecule was evaluated for their activity against human carcinoma cell lines. Comparison of cytostatic activities of the title molecule against acute lymphoblastic leukemia (Molt-4), colon carcinoma (HCT 116 and SW 620), breast carcinoma (MCF-7) and lung carcinoma (H 460) cell lines showed that demethoxylation caused the absence of inhibitory effect of novel 2,4-pyrimidinedione derivative 6-(3,3,4,4,4-pentafluoro-2-hydroxy-1-butenyl)-2,4-pyrimidinedione [9]. In previous publication, the title molecule was synthesized and characterized with X-ray diffraction method, and its structure was elucidated with ^{1}H, ^{13}C, and ^{19}F NMR spectra and IR spectra by Krištafor et al. [9]. To the best of our knowledge, the theoretical calculations of conformational, natural bond orbital (NBO) and nonlinear optical (NLO) analysis, molecular geometry, vibrational modes, molecular frontier orbital energy, electronic and thermodynamic properties of the title molecule have been not investigated yet. The purpose of this study is to eliminate this deficiency observed in the literature. With this aim, the theoretical calculations on structural, spectroscopic, electronic and electric properties of title molecule have been performed by using HF and DFT/B3LYP methods.

COMPUTATIONAL DETAILS

The molecular structure of the title molecule in the ground state (in vacuo) is computed by performing both Hartree-Fock (HF) and the density functional theory (DFT) by a hydrid functional B3LYP (Becke's three parameter hybrid functional using the LYP cor-

[1] The article is published in the original.

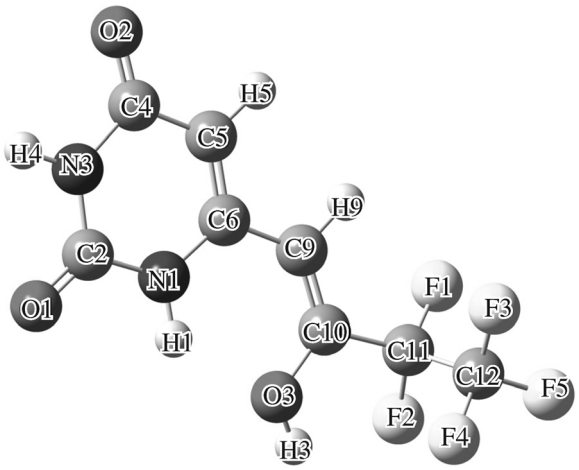

Fig. 1. The theoretical geometric structure of the title molecule obtained from B3LYP level.

relation functional) methods [10, 11] at 6-311++G(*d,p*) level. The optimized geometrical parameters and vibrational frequencies were calculated at the same computational levels. Conformational analysis were performed for τ_1(O3–C10–C11–C12), τ_2(C10–C9–C6–N1), and τ_3 (C10–C9–C6–C5) dihedral angles by using HF/6-31G(*d,p*) level. ^{1}H NMR and ^{13}C NMR chemical shifts are calculated within the gauge-independent atomic orbital (GIAO), individual gages for atoms in molecules (IGAIM) and continuous set of gage transformations (CSGT) methods applying B3LYP level. The NBO analysis was performed to investigate the intra and intermolecular bonding and interaction among bonds and charge transfer or conjugative interactions in the title compound. B3LYP level was also used to calculate the dipole moment (μ), the mean polarizability ($\langle\alpha\rangle$), the anisotropy of the polarizability ($\Delta\alpha$), and the total first static hyperpolarizability ($\langle\beta\rangle$). All calculations were performed by using Gaussian 09 program package [12] and the visualization parts of results were done with GaussView 5 program [13]. Additionally, harmonic vibrational frequencies for the title molecule are scaled by 0.9555 for HF and 0.9970 for B3LYP in order to correct the well-known systematic errors [14].

Table 1. Longitudinal component of the total static dipole moment (μ), the mean polarizability ($\langle\alpha\rangle$), the anisotropy of the polarizability ($\Delta\alpha$), and the mean first ($\langle\beta\rangle$) hyperpolarizability of the title molecule (obtained at B3LYP/6-311++G(*d,p*) level)

Parameter	Value	Parameter	Value
μ_x	−4.6083 D	β_{xxx}	−120.6565882 a.u.
μ_y	0.8259 D	β_{xyy}	105.4080537 a.u.
μ_z	−0.9568 D	β_{xzz}	−8.9948328 a.u.
μ	4.7785 D	β_{yyy}	−161.6451785 a.u.
α_{xx}	186.3042534 a.u.	β_{xxy}	102.5970827 a.u.
α_{yy}	137.4925641 a.u.	β_{yzz}	−37.5977946 a.u.
α_{zz}	76.2911952 a.u.	β_{zzz}	34.5562501 a.u.
$\langle\alpha\rangle$	133.3626709 a.u.	β_{xxz}	−22.1910218 a.u.
$\Delta\alpha$	95.47529 a.u.	β_{yyz}	31.0378696 a.u.
$\langle\alpha\rangle$	19.7645×10^{-24} esu	$\langle\beta\rangle$	108.6830 a.u.
$\Delta\alpha$	14.1494×10^{-24} esu	$\langle\beta\rangle$	938.9453×10^{-33} esu

RESULTS AND DISCUSSION

Geometrical Structure

The optimized geometry of the title molecule was calculated by using HF and DFT/B3LYP with 6-311++G(*d,p*) basis set, and the theoretical geometric structure of the title molecule obtained from B3LYP level is given in Fig. 1. The title molecule was synthesized by Krištafor et al. [9], but the crystal structure parameters such as bond lengths and angles were not presented. So, experimental parameters of the analogous molecule, 6-(3,3,4,4,4-pentafluoro-2-hydroxy-1-butenyl)-2,4-dimethoxypyrimidine, were selected to compare with the theoretical bond lengths, bond angles and dihedral angles obtained from DFT/B3LYP and HF methods. The crystal structure of the analogous of title molecule was taken from Cambridge Crystallographic Data Center (CCDC 685948), and compared with the theoretical results in Table 1. When compared to experimental results [9], theoretical methods estimate systematically longer bond lengths. However, it should be noted that the experimental results belong to solid phase and the theoretical calculations belong to gas phase.

The O3–C10 bond length was found at 1.319 Å [9] and this bond is calculated to be at 1.3447 and 1.3608 Å using HF and B3LYP methods with 6-311++G(*d,p*) basis set, respectively. The N1–C6 bond length observed at 1.363 Å [9] is calculated to be at 1.3754 Å and 1.3820 Å using HF and B3LYP methods, respectively. The C6–C9 and C10–C11 bond lengths were found at 1.439 and 1.514 Å [9], and these bond lengths are calculated as 1.4710 and 1.5160 Å for HF, 1.4574 and 1.5161 Å for B3LYP level. The O1–C2 and O2–C4 bond lengths were calculated as 1.1897 and 1.1902 Å for HF, 1.2127 and 1.2169 Å for B3LYP level. These bond lengths showed the double bond character of C=O bond. The N3–C4–O2 bond angle observed as 118.70° [9] has been calculated as 120.83° and 120.58° using HF and B3LYP level. The O3–C10–C9 bond angle was found at 126.80° [9], and this angle has been calculated at 124.07° and 123.35° by using HF and B3LYP, respectively.

Conformational Analysis

The minimum point structures located on the potential energy surface (PES) scan of the title molecule submitted to optimization using HF/6-31G(*d*,*p*) level were performed in the gas phase. From the rotation of different groups, the minimum energy conformations are obtained. In order to reveal all possible conformations of the title molecule, detailed potential energy curves for τ_1(O3–C10–C11–C12), τ_2(C10–C9–C6–N1), and τ_3 (C10–C9–C6–C5) dihedral angles were performed in steps of 10° from 0° to 360° and one dimensional PES scan for the title molecule were presented in Fig. 2. Structure of highest and lowest energy conformers for τ_1, τ_2, and τ_3 dihedral angles and the computed energy values of these dihedral angles are given in Fig. 3. These minimum energy curves for τ_1(O3–C10–C11–C12) dihedral angles have been obtained at ~78.85° and 81.15° as shown in Fig. 3. It is clear that 81.15° corresponds to the local minimum energy calculated as ~1136.1311 Hartree, and ~78.85° corresponds to the global minimum energy calculated as ~1136.1312 Hartree. Figure 3 shows that 0.37° corresponds to the global minimum point while 189.63° corresponds to the local minimum point for τ_2 (C10–C9–C6–N1) dihedral angle. These global and local minimum energies were calculated as ~1136.1312 and –1136.1242 Hartree, respectively. In Fig. 3, it is also demonstrated that 180.40° corresponds to the global minimum energy calculated as –1136.1312 Hartree and 370.40° corresponds to the local minimum energy calculated as ~1136.1242 Hartree for τ_3 (C10–C9–C6–C5) dihedral angle. Conformers resulting from unconstrained optimizations of the highest and the lowest energy structures of the contour plot of energy surfaces calculated by HF/6-31G of the title molecule are shown in Fig. 4.

Natural Bonding Orbital Analysis

The natural bonding orbital (NBO) analysis provides an efficient method for studying intra and intermolecular bonding and interaction among bonds, and also enables a convenient basis for investigating charge transfer or conjugative interaction in molecular systems. NBO analysis [15, 16] was used as a technique for studying hybridization and covalency effects in polyatomic wave functions. NBO calculations have been performed by using at B3LYP/6-311++G(*d*,*p*) levels in order to understand various second-order interactions between the filled orbitals of one subsystem and vacant orbitals of another subsystem, which are a measure of the intermolecular delocalization or hyperconjugation. A useful aspect of the NBO method is that it gives information about interactions in both filled and virtual orbital spaces, which could enhance the analysis of intra and intermolecular interactions [17, 18].

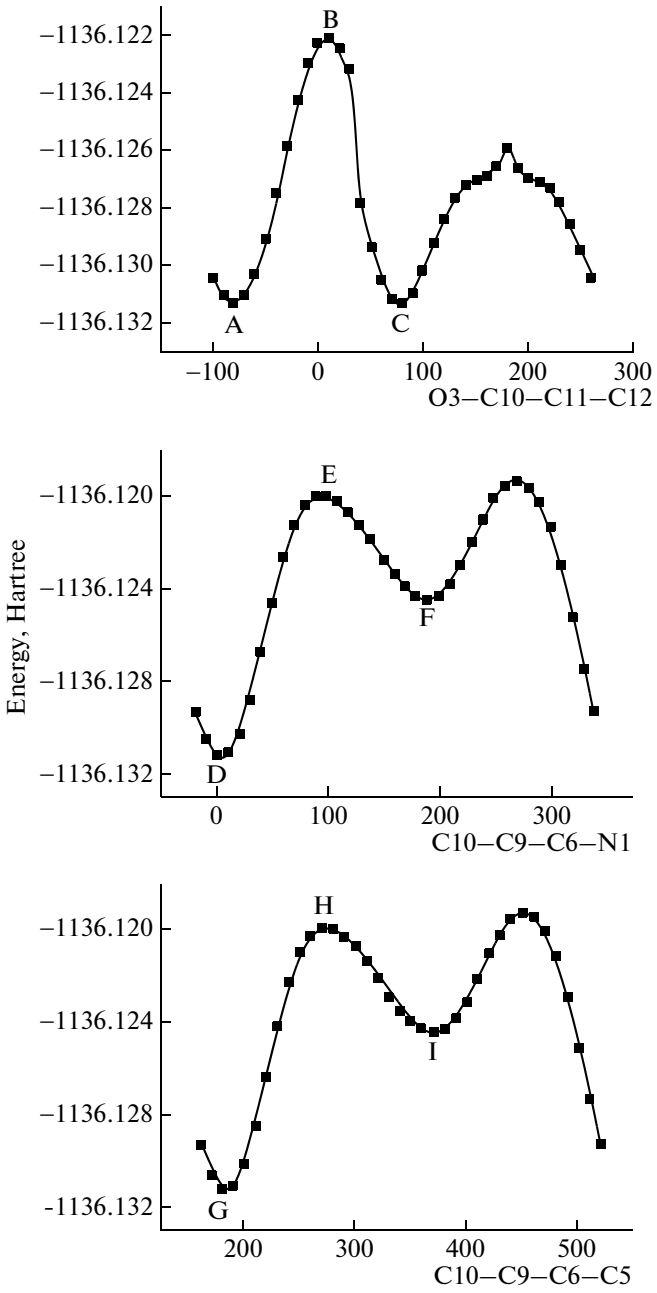

Fig. 2. One-dimensional potential energy surface (PES) scan of the calculated relative energies vs dihedral angles (τ) using HF/6-31G(*d*,*p*) of the title molecule.

The second-order Fock matrix was used to evaluate the donor–acceptor interactions in the NBO basis [16]. The interactions result in a loss of occupancy from the localized NBO of the idealized Lewis structure into an empty non-Lewis orbital. For each donor (*i*) and acceptor (*j*), the stabilization energy $E(2)$ associated with the delocalization $i \longrightarrow j$ is estimated as [19]

$$E(2) = \Delta E_{ij} = q_i F(i,j)^2/(\varepsilon_j - \varepsilon_i'),$$

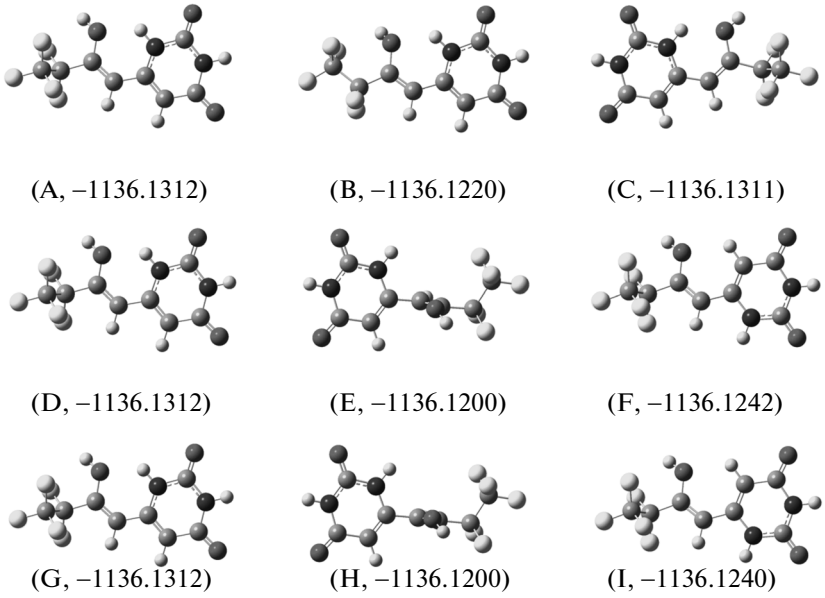

Fig. 3. Highest and lowest energy conformations using HF/6-31G(*d*,*p*) of the title molecule (*E*, Hartree).

where q_i is the donor orbital occupancy, ε_i and ε_j are diagonal elements and $F(i, j)$ is the off-diagonal NBO Fock matrix element. N_1 bond hybrid of the N1–C2 bond gains 34% in s character and 65.95% in *p* character (with hybrid orbital $sp^{1.94}$). In NBO analysis, the larger $E(2)$ values imply the intensive interaction between electron-donors and electron-acceptors, and greater the extent of conjugation of the whole system. In NBO analysis, the hyperconjugative $\sigma \longrightarrow \sigma^*$ interactions play a highly important role. These interactions represent weak departures from a strictly localized natural Lewis structure that constitutes the primary "non-covalent" effects. The results of NBO analysis indicate that there are strong hyperconjugative interactions σ (N1–C6) $\longrightarrow$ σ^* (O1–C2), σ (N1–C6) $\longrightarrow$ σ^* (O6–C9), and σ (C5–H5) $\longrightarrow$ σ^* (N3–C4) for the title molecule where appear to be at 2.07, 2.45, and 3.29 kcal/mol with B3YLP level, respectively. The second-order perturbation theory analysis of Fock matrix in NBO basis shows strong intramolecular hyperconjugative interactions of electrons. The interaction energies of π (C5–C6) $\longrightarrow$ π^* (O2–C4), π (C9–C10) $\longrightarrow$ π^* (F2–C11), and LP1 (N1) $\longrightarrow$ π^* (O1–C2) were calculated as 22.60, 3.34, and 53.52 kcal/mol for B3LYP level of DFT method, respectively. These interactions resulted in intramolecular charge transfer causing stabilization of the title molecule, and the large interaction energies (E) values are indicator of the weakening the respective bonds.

Polarizabilities and Hyperpolarizabilities

The polarizabilities and hyperpolarizabilities characterize the response of a system in an applied electric field [20, 21]. Electric polarizability is a fundamental characteristic of atomic and molecular systems [21]. Polarizabilities and hyperpolarizabilities could determine not only the strength of molecular interactions (such as the long-range intermolecular induction, dispersion forces, etc.) as well as the cross sections of different scattering and collision processes, but also the nonlinear optical properties of the system [22]. The theory of electric polarizability is a key element of the rational interpretation of a wide range of phenomena, from nonlinear optics [23] and electron scattering [24] to phenomena induced by intermolecular interactions [25] which reads to be

$$E = E^0 - \mu_\alpha F_\alpha - (1/2)\alpha_{\alpha\beta}F_\alpha F_\beta - (1/6)\beta_{\alpha\beta\gamma}F_\alpha F_\beta F_\gamma - (1/24)\gamma_{\alpha\beta\gamma\delta}F_\alpha F_\beta F_\gamma F_\delta + \ldots,$$

where E° is the energy of the free molecule, F_α is the field at the origin and μ_α, $\alpha_{\alpha\beta}$, $\beta_{\alpha\beta\gamma}$, and $\gamma_{\alpha\beta\gamma\delta}$ are the components of dipole moment, polarizability, the first-order hyperpolarizabilities and the second-order hyperpolarizabilities, respectively. In this paper, we present the values of the total static dipole moment (μ), the mean polarizability ($\langle\alpha\rangle$), the anisotropy of the polarizability ($\Delta\alpha$) and the mean first-order hyperpolarizability ($\langle\beta\rangle$) as defined [26, 27] in the following equation:

$$\mu = (\mu_x^2 + \mu_y^2 + \mu_z^2)^{1/2},$$

$$\langle\alpha\rangle = (\alpha_{xx} + \alpha_{yy} + \alpha_{zz})/3,$$

$$\Delta\alpha = ([(\alpha_{xx} - \alpha_{yy})^2 + (\alpha_{yy} - \alpha_{zz})^2 + (\alpha_{zz} - \alpha_{xx})^2]/2)^{1/2},$$

$$\langle\beta\rangle = (\beta_x^2 + \beta_y^2 + \beta_z^2)^{1/2},$$

where

$$\beta_x = \beta_{xxx} + \beta_{xyy} + \beta_{xzz}, \quad \beta_y = \beta_{yyy} + \beta_{xxy} + \beta_{yzz}$$
$$\beta_z = \beta_{zzz} + \beta_{xxz} + \beta_{yyz}.$$

The total static dipole moment, the mean polarizability, the anisotropy of the polarizability, the mean first-order and second-order hyperpolarizability have been calculated for the title molecule using DFT/B3LYP with the 6-311++G(*d*,*p*) basis set. The α and β components of GAUSSIAN 09 output are reported in atomic units and therefore the calculated values are converted into electrostatic units (α: 1 a.u. = 0.1482×10^{-24} esu and β: 1 a.u. = 8.6393×10^{-33} esu) and given in Table 1. According to the present calculations, the total molecular dipole moment, polarizability, anisotropy of the polarizability and first-order hyperpolarizability have been calculated as 4.7785 Debye, 19.7645×10^{-24}, 14.1494×10^{-24}, and 938.9453×10^{-33} esu at B3LYP/6-311++G(*d*,*p*) level for the title molecule, respectively. Additionally, from the tabulated values, it is noticed that hyperpolarizability is higher in the β_{yyy} direction due to the delocalization of charge cloud. The maximum β value is due to intermolecular hydrogen bonds and π–π stacking interactions.

Vibrational Spectra Analyses

We have not found any theoretical results for the vibrational spectrum of the title molecule in the literature, so we have calculated the theoretical vibrational spectra of title compound by using HF and B3LYP methods with the 6-311++G(*d*,*p*) basis set. In quantum chemistry calculations, all the vibrational frequencies are overestimated and in agreement with 10–20% of average error established for these calculations. It is well known that overestimation is higher in high wavenumber regions. As moved toward the low wavenumber regions, calculated vibration frequencies gets closer to experimental ones [28–30]. This overestimation depends on the type of vibrational mode and wavenumber range. DFT methods predict the wavenumbers which relatively close to the experimental ones, and B3LYP is one of the most used DFT level for this purpose. All calculated wavenumbers were scaled by using scaling factors as 0.9555 and 0.9970 [14] for HF/6-311++G(*d*,*p*) and B3LYP/6-311++G(*d*,*p*) methods, respectively. The bands calculated in the measured region 4000–400 cm^{-1} arise from the vibrations of O–H, N–H stretching, the internal vibrations and the vibrations of the lattice of the title molecule. Theoretical and experimental vibrational wavenumbers for the title molecule are listed in Table 2. Most of the observed bands in infrared spectra of the title molecule belong to phenyl and hydroxyphenyl groups' modes; only some of them may be assigned to ring C–H and C–C stretching vibrations. Some of these bands have been calculated (with HF/6-311++G(*d*,*p*))

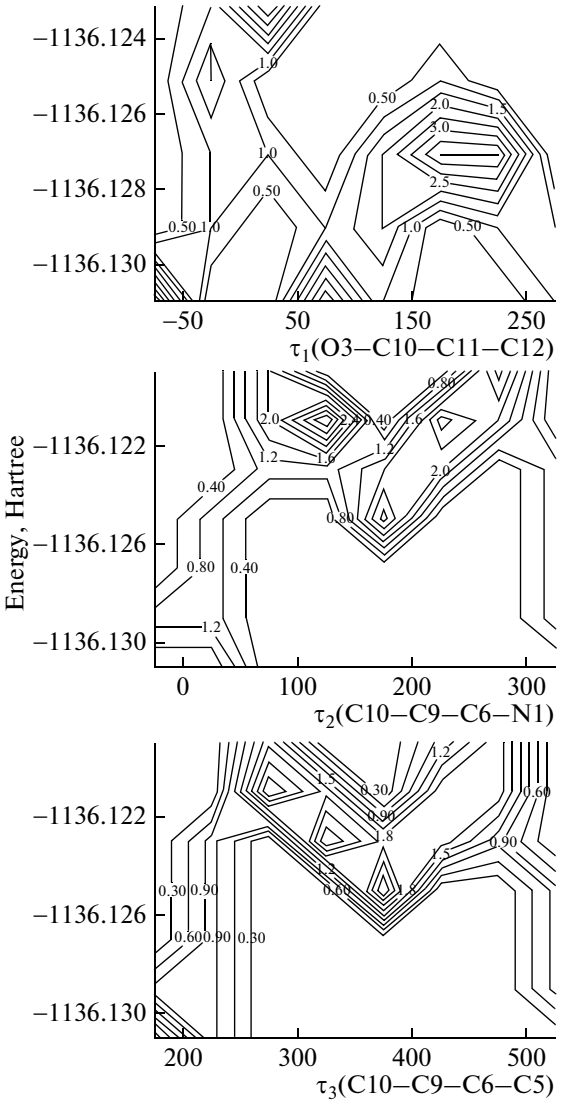

Fig. 4. Contour plot of energy surfaces using HF/6-31G(*d*,*p*) of the title molecule.

at 3248, 3238, and 1433 cm^{-1} for the title molecule. Other essential characteristic vibrations of the title molecule are O–H, C=C, C=C–H, N–H, C–F, C=O stretching vibrations. The O–H, C=O, and C–F stretching were observed at 3391, 1668, and 754 cm^{-1} [9] for the title molecule, respectively. These modes have been calculated at 3786, 1752, and 614 cm^{-1} for the title molecule with B3LYP/6-311++G(*d*,*p*) level. The other assignment of internal vibrations of the title molecule can be seen in Table 2. Additionally, the calculated infrared (IR) and Raman spectra of the title molecule are shown in Figs. 5a and 5b, respectively.

NMR Spectra Analyses

In this study, ^1H and ^{13}C NMR chemical shifts were calculated within the gage-including atomic orbital

Table 2. Comparison of the observed (IR) and calculated (I, HF/6-311++G(*d*,*p*), II, B3LYP/6-311++G(*d*,*p*)) vibrational wavenumbers and assignments for the title molecule

Assignments	IR [9]	I	II	Assignments	IR [9]	I	II
ν(O–H)	3391	3957	3786	ρ(C=C–H)	–	1063	1076
ν(N–H)	–	3700	3594	τ(N–C–N)	–	1044	1048
ν(N–H)	3014	3671	3588	τ(N–C–N)	–	970	1015
ν(C–H)	–	3248	3227	$(C=C-H)_{bend}$	1155	941	945
ν_a(C–H)	–	3238	3210	$(C=C-H)_{bend}$	1033	868	875
ν(C=O)	–	1880	1792	$(C=C-H)_{bend}$	1005	861	818
ν(C=O)	1668	1863	1752	$(N-C-N)_{bend}$	–	812	752
ν(C=C), ν(C=O)	–	1836	1726	τ(C–F3)	–	785	740
ν(C=C), ν(C=O)	1601	1723	1632	$(C=C-H)_{bend}$	807	766	725
ν(C–N)	1539	1594	1522	$(C-C-H)_{bend}$	–	735	694
ρ(N–H)	–	1492	1413	$(C=C-H)_{bend}$	680	700	684
ρ(N–H)	–	1477	1401	$\tau(C-N-C)_{ring}$	–	683	655
ρ(C=C–H)	1443	1463	1391	w(N–H)	–	650	631
ν(C–C)	1395	1433	–	w(N–H), δ(C–F3)	754	632	614
ρ(N–H), ρ(C–H)	1324	1425	1359	$\rho(C-C-H)_{ring}$	–	617	591
ρ(C=C–H), ρ(O–H)	–	1363	1306	$\tau(C-N-C)_{ring}$	–	576	548
ν(C–C)	–	–	1293	w(N–H), δ(C–F2), δ(C–F3)	–	569	535
ρ(O–H), ν_a(C–F3)	–	1333	–	$(C=C-O)_{bend}$, w(N–H), δ(C–F3)	–	554	526
ρ(C=C–H), ρ(O–H)	–	1299	–	$\delta(C-C-N)_{ring}$	–	539	519
ν(C–N), ρ(C–H)	–	1284	–	δ(C–F3), δ(C–F2)	–	506	481
ν_a(C–F2), ρ(C–H), ρ(O–H)	–	1271	1225	t(C–F), w(O–H)	–	382	348
ρ(C–H), ρ(N–H), ρ(O–H)	–	1149	1212	w(O–H)	–	323	328
ν_a(C–F3), ρ(C–H)	–	–	1194	t(C–F2), t(C–F3)	–	277	306
ν(C–N)	–	1091	1190	t(C–F2), t(C–F3)	–	258	266
ν_a(C–F3), ρ(O–H)	–	–	1182	t(C–F2), t(C–F3)	–	229	248
ν_a(C–F2), ρ(C–H)	–	–	1146	Lattice	–	196	221

Vibrational modes: ν, stretching; a, asymmetric; s, symmetric; ρ, rocking; δ, scissoring; w, wagging; t, twisting; τ, torsion.

(GIAO), individual gages for atoms in molecules (IGAIM) and continuous set of gage transformations (CSGT) methods applying B3LYP level with 6-311++G(*d*,*p*) basis set. A comparison of the experimental and theoretical spectra can be very useful in making correct assignments and understanding the basic relationship between chemical shift values and chemical environment of atoms. Correlation graphic of calculated and experimental ^{1}H NMR and ^{13}C NMR chemical shifts are shown in Fig. 6.

In Table 3, the experimental and the theoretical ^{1}H and ^{13}C isotropic chemical shifts (with respect to TMS, all values in ppm) for the title molecule has been given. The GIAO has been shown to provide results that are often more accurate than those calculated with other approaches, at the same basis set size [23]. It is well known that aromatic carbons give signals in the range of 100–150 ppm. However, C4, C6, and C2 atoms give peaks at 164.99, 155.68, and 151.68 ppm [9]. These peaks were calculated at 164.83, 149.80, and 151.95 by GIAO approach. These shifts are originated from electronegativity properties of N and O atoms attached to C4, C2, and C6. Such effects of chemical shifts are very well known in the literature [31]. The ^{13}C chemical shift values for all calculations have range from ~164.83 to ~127.40 ppm, while the ^{1}H chemical shift values for all calculations have range from ~8.20 to ~5.27 ppm at B3LYP/6-311++G(*d*,*p*) level in the average for title compound. As can be seen from Table 3, the theoretical ^{1}H and ^{13}C chemical shift results of the title molecule are in an agreement with the experimental ^{1}H and ^{13}C chemical shift data.

Frontier Molecular Orbitals

The highest occupied molecular orbital (HOMO) and the lowest unoccupied molecular orbital (LUMO) are very popular quantum chemical parameters. These

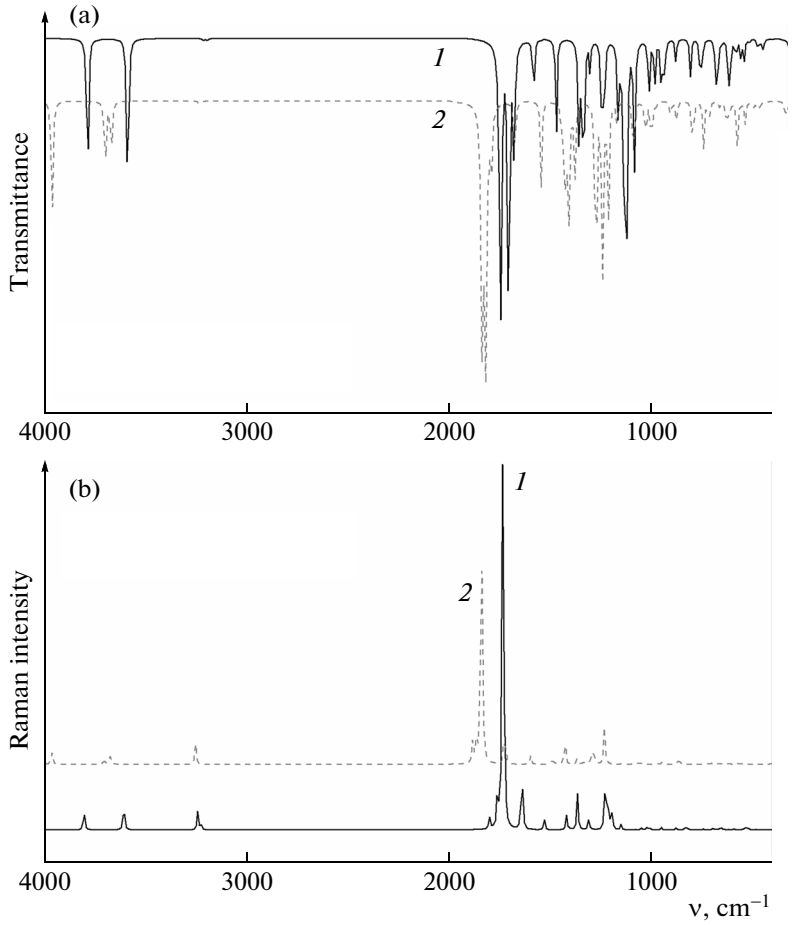

Fig. 5. The calculated (a) IR and (b) Raman spectra of the title molecule; *1*, B3LYP/6-311++G(*d*,*p*); *2*, HF/6-311++G(*d*,*p*).

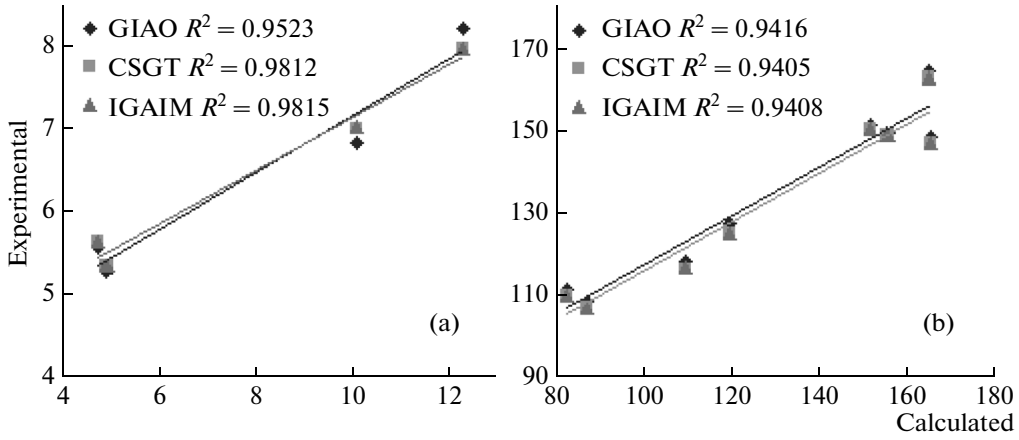

Fig. 6. Correlation graphic of experimental and calculated by B3LYP/6-311++G(*d*,*p*) level (a) ^{1}H and (b) ^{13}C chemical shifts (ppm) of the title molecule.

molecular orbitals are also called the frontier molecular orbitals (FMOs), and determine the way in which a molecule interacts with other species. The FMOs are important in determining molecular reactivity and the ability of a molecule to absorb light. The HOMO is the orbital that can act as an electron donor, since it is the outermost (higher energy) orbital containing electrons. On the other hand, LUMO can be thought the

Table 3. The calculated (obtained at B3LYP/6-311++G(*d*,*p*) level) and experimental ^{13}C and ^{1}H isotropic NMR chemical shifts for the title molecule

Atom	Experimental	GIAO	CSGT	IGAIM
^{1}H				
H5	4.91	5.27	5.35	5.35
H9	4.77	5.57	5.63	5.63
H2	12.29	8.20	7.96	7.97
H4	10.12	6.84	7.02	7.03
^{13}C				
C4	164.99	164.83	163.37	163.38
C6	155.68	149.80	149.44	149.44
C2	151.68	151.95	150.78	150.78
C5	87.170	108.39	107.05	107.03
C9	82.960	111.13	109.89	109.88
C10	165.17	148.80	147.46	147.47
C11	109.38	118.20	116.41	116.46
C12	119.50	127.40	125.13	125.19

Table 4. The calculated (I, HF/6-311++G(*d*,*p*), II, B3LYP/6-311++G(*d*,*p*)) total molecular energies, frontier orbital energies, electronegativity, hardness and softness for the title molecule

Parameters	I	II
E_{HOMO}, eV	−6.8617	−7.1188
E_{LUMO}, eV	−2.5347	−2.8254
$\Delta E = E_{LUMO} - E_{HOMO}$, eV	4.3270	4.2934
I, eV	6.8617	7.1188
A, eV	2.5347	2.8254
χ, eV	4.6982	4.9721
η, eV	2.1635	2.1467
S, eV^{-1}	0.2311	0.2329
E_{total}, eV	−1136.8944	−1142.6235

innermost orbital containing free places to accept electrons [32, 33]. The energy of the HOMO is directly related to the ionization potential, while LUMO energy is directly related to the electron affinity. Energy difference between HOMO and LUMO orbital is called as energy gap that is an important stability for structures [34]. The total energy, HOMO and LUMO energies, the energy gap (ΔE), the ionization potential (I), the electron affinity (A), the absolute electronegativity (χ), the absolute hardness (η), and softness (S) for the title molecule have been calculated at HF and DFT/B3LYP level in the 6-311++G(*d*,*p*) basis set, and the obtained results are given in Table 4. The calculated HOMO and LUMO energies show that charge transfer occurs within the molecule.

By using HOMO and LUMO energy values for a molecule, electronegativity and chemical hardness can be calculated as follows: $\chi = (I + A)/2$ (electronegativity), $\eta = (I - A)/2$ (chemical hardness) $S = 1/2\eta$ (chemical softness), where I and A are ionization potential and electron affinity, $I = -E_{HOMO}$ and $A = -E_{LUMO}$, respectively [35–37].

Surfaces for the frontier orbitals were drawn to understand the bonding scheme of present compound. The contour plots of the highest occupied and the lowest unoccupied molecular orbitals using B3LYP/6-311G(*d*,*p*) method were given in Fig. 7. The coefficients of Frontier α-spin molecular orbitals for title compound using B3LYP/6-311++G(*d*,*p*) level are calculated as follows:

$$\varphi_{HOMO} \approx -0.13 \times 2p_z^{N1} + 0.02 \times 3p_x^{N1} - 0.02 \times 3p_z^{N3} - 0.02 \times 4p_z^{N3} + 0.14 \times 3p_z^{O1} - 0.11 \times 2p_z^{O2} + 0.13 \times 4p_z^{O3} - 0.01 \times 2p_y^{F2} - 0.02 \times 3p_y^{F2} + 0.01 \times 2p_y^{F1} - 0.03 \times 4s^{F1} - 0.01 \times 3p_x^{F4} + 0.01 \times 4p_z^{F4} - 0.02 \times 3p_z^{C2} + 0.01 \times 3p_z^{C4} - 0.03 \times 4p_z^{C4} - 0.02 \times 2p_x^{C5} + 0.16 \times 2p_z^{C5} - 0.01 \times 2p_x^{C6} - 0.08 \times 2p_z^{C6} - 0.04 \times 2p_x^{C9} - 0.06 \times 3p_x^{C9} - 0.08 \times 2p_z^{C10} - 0.13 \times 3p_z^{C10} + 0.01 \times 3s^{C11} + 0.02 \times 3s^{C12},$$

$$\varphi_{LUMO} \approx + 0.06 \times 2p_z^{N1} + 0.09 \times 3p_z^{N1} - 0.06 \times 2p_z^{N3} + 0.01 \times 3p_x^{N3} - 0.02 \times 2p_z^{O1} - 0.08 \times 2p_z^{O2} + 0.04 \times 4p_x^{O3} + 0.04 \times 2p_y^{F2} + 0.06 \times 3p_y^{F2} - 0.01 \times 2s^{F1} + 0.12 \times 4s^{F1} - 0.02 \times 3p_y^{C4} - 0.03 \times 4p_y^{C4} + 0.02 \times 3p_z^{C2} + 0.06 \times 2p_z^{C4} + 0.11 \times 3p_z^{C4} - 0.11 \times 2p_z^{C5} + 0.18 \times 3p_z^{C5} - 0.10 \times 2p_z^{C6} - 0.17 \times 3p_z^{C6} - 0.11 \times 2p_x^{C9} - 0.03 \times 3p_x^{C9} + 0.15 \times 2p_z^{C10} + 0.25 \times 3p_z^{C10} + 0.10 \times 3p_z^{C11} - 0.06 \times 3s^{C12}.$$

Analysis of Molecular Electrostatic Potential Surfaces

The molecular electrostatic potential (MEP) has been established extensively as a useful quantity to explain hydrogen bonding, reactivity and structure activity of molecular behaviors. We calculated the molecular electrostatic potential (MEP) and the contour map of molecular electrostatic potential surface and discussed their distributions. The 3D plot of MEP using DFT/6-311++G(*d*,*p*) method for title compound is given in Fig. 8. The MEP which is a method of mapping electrostatic potential onto the iso-electron density surface simultaneously displays electrostatic potential (electron + nuclei) distribution, molecular shape, size and dipole moments of the mol-

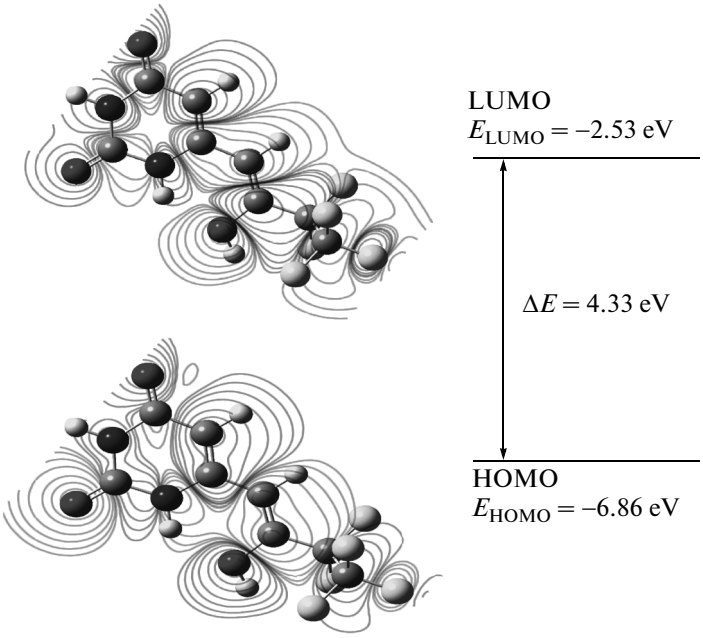

Fig. 7. The energies and contour plots of frontier molecular orbitals using B3LYP/6-311G(*d*,*p*) method for the title molecule.

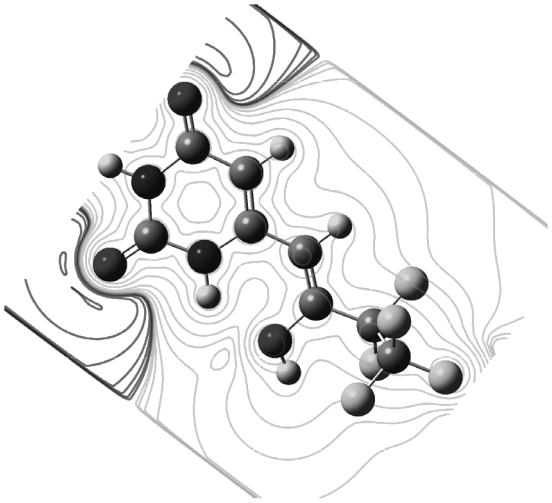

Fig. 8. The contour plot of ESP obtained using B3LYP/6-311G(*d*,*p*) level of the title molecule.

ecule and it provides a visual method to understand the relative polarity [38]. According to simulated molecular electrostatic potential, the negative region is mainly localized over the oxygen atoms of carbonyl group, indicating a possible site for electrophilic attack. The maximum positive region is localized on N–H bonds of the title molecule, indicating a possible site for nucleophilic attack. These sites give information about the region from where the compound can have intermolecular interactions. The molecular electrostatic potential ESP correlates the total charge distribution with dipole moments, partial charges, electronegativity and site of chemical reactivity of a molecule. The simulated ESP is given in Fig. 8.

Mulliken, Atomic Polar Tensor (APT), Natural (NBO) Charge Analysis

Atomic charges and charge transfer are used as a concept in chemical reasoning about molecular

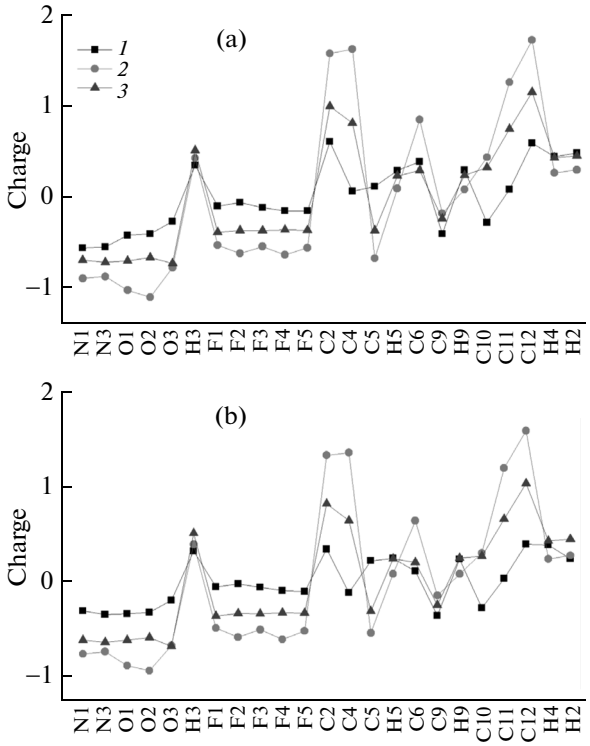

Fig. 9. Comparative of (*1*) Mulliken, (*2*) APT, and (*3*) NBO plots of the title molecule; (a) HF/6-311++G(*d*,*p*), (b) DFT/B3LYP/G-311++G(*d*,*p*).

behavior and reactivity. Thus, atomic charges continue to play an important role in quantum chemistry and much research continues to being done to refine the concept of an atomic charge. Since the description of charge populations of atomic orbitals by Mulliken [39] are widely used tools for the interpretation of the internal structure of molecular orbitals. It is clear that Mulliken populations yield one of the simplest pictures of charge distribution and Mulliken charges render net atomic populations in the molecule [40]. Atomic Polar Tensor (APT) charge is interpreted as sum of charge tensor and charge flux tensor, leading to a charge-charge flux model [41]. The APT charges [42] are independent of the basis sets used in the calculations while the Mulliken charges depend on the basis sets. The Mulliken, NBO and APT charge distributions of the title molecule has been calculated at HF/6-311++G(*d*,*p*) and B3LYP/6-311++G(*d*,*p*) levels of theory. The results are given in Fig. 9. As can be seen from the Fig. 9, the magnitudes of the carbon Mulliken charges, found to be either positive or negative, were noted to change from –0.414508 to 0.595562 for title compound. Since the C2 and C4 atom bound to electronegative oxygen atoms, these carbon atoms have higher positive charge than other carbons. The H3 atom exhibits the largest positive charge among hydrogen atoms due to the bounding to O atom. The Mulliken charges show a behavior similar to that of the APT and NBO charges. It is found that all nitrogen and oxygen atoms accumulate negative charges as a result of molecular relaxation.

CONCLUSIONS

In this study, molecular structure, conformation study, Natural Bonding Orbital (NBO) analysis harmonic vibrational frequencies, ^{1}H and ^{13}C NMR chemical shifts, HOMO and LUMO energy analysis, electronegativity (χ), hardness (η), softness (S), molecular electrostatic potential maps (MEP), Mulliken charges and atomic polar tensor-based charges, the natural bonding orbital (NBO), electric dipole moment (μ), polarizability (α), the first-order hyperpolarizability (β) and second-order hyperpolarizability (γ), electronic and thermodynamic properties of the title molecule have been calculated by using HF/6-311++G(*d*,*p*) and B3LYP/6-311++G(*d*,*p*) methods. Three possible conformers were obtained based on the PES scan method as a function of the dihedral angles, τ_1(O3–C10–C11–C12), τ_2 (C10–C9–C6–N1), and τ_3 (C10–C9–C6–C5). The small differences were observed between the theoretical and experimental structural parameters and vibrational wavenumbers. However, it should be noted that the experimental section was performed in solid phase while theoretical calculations were performed in gas phase. NBO analysis was carried out by B3LYP method in detail. NBO analysis indicated that there are strong hyperconjugative interactions resulted in intramolecular charge transfer causing stabilization of the title compound. Nonlinear optical behavior of the examined compound was investigated by the determination of the electric dipole moment μ, the polarizability α and the hyperpolarizability β using B3LYP methods. So, it is demonstrated that the investigated compound can be used as a NLO material.

REFERENCES

1. P. Das, C. P. Spears, A. H. Shahinian, S. K. Dasgupta, et al., Bioorg. Med. Chem. Lett. **6**, 2477 (1996).
2. M. Baba, E. de Clercq, H. Tanaka, et al., Mol. Pharmacol. **39**, 805 (1991).
3. J. Balzarini, A. Karlsson, and E. de Clercq, Mol. Pharmacol. **44**, 694 (1993).
4. A. Mai, M. Artico, G. Sbardella, et al., J. Med. Chem. **40**, 1447 (1997).
5. S. Prekupec, D. Makuc, J. Plavec, et al., Antiviral Chem. Chemother. **16**, 327 (2005).
6. S. Prekupec, D. Makuc, J. Plavec, et al., J. Med. Chem. **50**, 3037 (2007).
7. P. Pospisil, D. B. Pilger, S. Marveggio, et al., Helv. Chim. Acta **85**, 3237 (2002).
8. T. Kulikowski, Pharm. World Sci. **16**, 127 (1994).
9. S. Krištafor, T. Gazivoda, M. Cetina, et al., J. Mol. Struct. **923**, 19 (2009).
10. A. D. Becke, J. Chem. Phys. **98**, 5648 (1993).

11. C. Lee, W. Yang, and R. G. Parr, Phys. Rev. B **37**, 785 (1988).
12. M. J. Frisch, G. W. Trucks, H. B. Schlegel, et al., *Gaussian 09*, Revision A.1 (Gaussian, Inc., Wallingford CT, 2009).
13. R. Dennington, T. Keith, and J. Millam, *GaussView*, Version 5 (Semichem Inc., Shawnee Mission KS, 2009).
14. D. Avcı and Y. Atalay, Int. J. Quantum. Chem. **109**, 328 (2009).
15. J. P. Foster and F. Weinhold, J. Am. Chem. Soc. **102**, 7211 (1980).
16. A. E. Reed, L. A. Curtiss, and F. Weinhold, Chem. Rev. **88**, 899 (1988).
17. A. E. Reed, R. B. Weinstock, and F. Weinhold, J. Chem. Phys. **83**, 735 (1985).
18. F. Weinhold and C. R. Landis, *Valency and Bonding: A Natural Bond Orbital Donor-Acceptor Perspective* (Cambridge Univ. Press, Cambridge, 2005).
19. J. Chocholousova, V. V. Spirko, and P. Hobza, Phys. Chem. Chem. Phys. **6**, 37 (2000)
20. P. S. Kumar, K. Vasudevan, A. Prakasam, et al., Spectrochim. Acta A **77**, 45 (2010).
21. A. D. Buckingham, Adv. Chem. Phys. **12**, 107 (1967).
22. O. Christiansen, J. Gauss, and J. F. Stanton, Chem. Phys. Lett. **305**, 147 (1999).
23. N. Bloembergen, *Nonlinear Optics* (Benjamin, New York, 1965).
24. N. F. Lane, Rev. Mod. Phys. **52**, 29 (1980).
25. G Birnbaum, *Phenomena Induced by Intermolecular Interactions* (Plenum, New York 1980).
26. G. Maroulis, J. Chem. Phys. **5**, 113 (2000).
27. A. Başoğlu, D. Avcı, Y. Atalay et al., Spectrochim. Acta A **79**, 1425 (2011).
28. A. P. Scott and L. Radom, J. Phys. Chem. **100**, 16502 (1996).
29. M. A. Palafox, M. Gill, N. J. Nunez, V. K. Rastogi, L. Mittal, and R. Saharma, Int. J. Quant. Chem. **103**, 394 (2005).
30. D. Avcı and Y. Atalay, Int. J. Quantum Chem. **109**, 328 (2009).
31. M. R. Del Giudice, G. Settimj, et al., Tetrahedron **40**, 4087 (1984).
32. S. Güner, Y. Atalay, and A. Dolma, Spectrochim. Acta A **934**, 389 (2011).
33. G. Gece, Corros. Sci. **50**, 2981 (2008).
34. K. Fukui, *Theory of Orientation and Stereoselection* (Springer, Berlin, 1975).
35. Y. Atalay, A. Başoğlu, and D. Avcı, Spectrochim. Acta A **69**, 460 (2008).
36. H. Pir, N. Günay, D. Avcı, et al., Spectrochim. Acta A **96**, 916 (2012).
37. H. Pir, N. Günay, Ö. Tamer, et al., Spectrochim. Acta A **112**, 331 (2013).
38. R. G. Pearson, Proc. Natl. Acad. Sci. **83**, 8440 (1986).
39. I. Fleming, *Frontier Orbitals and Organic Chemical Reactions* (Wiley, New York, 1976).
40. R. S. Mulliken, J. Chem. Phys. **23**, 1833 (1955).
41. V. Mukherjee, N. P. Singh, and R. A. Yadav, Spectrochim. Acta A **73**, 249 (2009).
42. J. F. Biarge, J. Herranz, and J. Morcillo, Ann. Fis. Quim. A **57**, 81 (1961).